Applied Thermal Engineering 220 (2023) 119578

Contents lists available at ScienceDirect

Applied Thermal Engineering

journal homepage: www.elsevier.com/locate/ate

Research Paper

Technoeconomic optimization of superalloy supercritical CO_2 microtube shell-and-tube-heat exchangers

Akshay Bharadwaj Krishna, Kaiyuan Jin, Portonovo S. Ayyaswamy, Ivan Catton, Timothy S. Fisher *

Mechanical and Aerospace Engineering Department, University of California Los Angeles (UCLA), Los Angeles, CA, 90095, USA

ARTICLE INFO

Keywords:
Supercritical CO_2
Shell-and-tube heat exchanger
Economic optimization
Cost model
Particle Swarm Optimization

ABSTRACT

Heat exchangers are critical components of aerospace systems and improve efficiency of operation by providing waste heat recovery. Supercritical CO_2 has emerged as a promising candidate working fluid due to its potential in increasing the power density of heat exchangers. In this paper, a generalized costing model is developed to estimate the capital costs incurred to manufacture microtube shell-and-tube heat exchangers. This model is utilized in conjunction with an accurate and efficient 2D numerical shell-and-tube heat exchanger performance prediction model to conduct optimization studies with two key objectives – minimization of cost and maximization of heat exchanger power density – on supercritical CO_2 microtube heat exchangers utilizing superalloy Haynes 282 as the solid material. A methodology is then demonstrated to optimize these heat exchangers using Particle Swarm Optimization for aerospace applications and highly compact and cost-effective optimal designs with power density around 20 kW/kg and cost per conductance less than 5 $\$ \cdot K/W$ are obtained.

1. Introduction

Heat exchangers enable significant waste heat recovery and efficient energy management in energy systems by facilitating the transfer of thermal energy between two fluids [1–3]. Shell-and-tube heat exchangers (STHXs) are the most common high-temperature and high-pressure heat exchangers [4] and microtube shell-and-tube heat exchangers (MT-STHXs) are promising new alternatives. STHXs are popular owing to their high effectiveness, versatility in operation, and low cost [5–7] but are generally heavier and occupy larger volumes due to the use of tubes with inner diameters larger than 5 mm. MT-STHXs are gaining interest as they exhibit all advantages of STHXs and are compact with high power densities [8]. The drawbacks of STHXs are mitigated in MT-STHXs by utilizing tubes of smaller inner diameters.

Working fluid selection is critical to achieving high thermal cycle efficiency, low carbon footprint, and compact size. Performance of nanofluids such as Al_2O_3/water, TiO_2/water, and MWNT-water in STHXs has been studied [9,10]. However, their impact on reliability of thermal systems and performance subject to elevated temperatures, pressures, and wear conditions of an in-the-loop turbine generator as in the present work remain unclear to us. All the benefits mentioned earlier can be realized by using supercritical CO_2 (sCO_2) as the working fluid [11–13]. Good chemical stability, high density at high temperatures, and a low critical point (7 MPa and 300 K) make sCO_2 a more attractive candidate fluid for operation in energy systems than other supercritical fluids [14–16]. Aside from selection of working fluids, the choice of solid material is crucial because the MT-STHX needs to withstand long duration of operation at elevated temperatures and pressures. Superalloys such as Haynes 282 are promising candidates due to their high creep strength at extreme operating conditions [17–19].

Developing accurate and computationally efficient models to predict thermohydraulic performance of heat exchangers is the first step towards obtaining optimal designs. A widely used modeling technique is Computational Fluid Dynamics (CFD), but this method can be computationally expensive [20–22]. Correlation-based approaches such as the Kern [23] and the Bell–Delaware [24] method are the other common prediction techniques, but the Kern method provides a rather conservative estimate of STHX performance while the Bell–Delaware method is not capable of providing detailed information about the temperature and flow fields. Correlation-based prediction approaches eliminate the complexity of the solution but require highly accurate thermohydraulic correlations to develop a high-fidelity MT-STHX performance prediction model. The above-mentioned drawbacks have been overcome by Krishna et al. by developing new, highly accurate correlations [25] and a computationally efficient numerical model [26,27]. The 2D model utilizes the concept of volume averaging and has been validated experimentally by Jin et al. [28].

* Corresponding author.
E-mail address: tsfisher@ucla.edu (T.S. Fisher).

https://doi.org/10.1016/j.applthermaleng.2022.119578
Received 9 August 2022; Received in revised form 5 October 2022; Accepted 24 October 2022
Available online 21 November 2022

Nomenclature

Variables

A_c	Cross-sectional free flow area between two tubes $[m^2]$
A_{HT}	Area of heat transfer $[m^2]$
c_1, c_2	Acceleration constants
C_{cap}	Capital cost of shell-and-tube heat exchanger [$]
D_E	Effective diameter [m]
D_f	Fin diameter [m]
D_h	Hydraulic diameter [m]
D_{it}	Tube inner diameter [m]
D_{ot}	Tube outer diameter [m]
f	Friction factor
gb	Global best location of the population
h	Heat transfer coefficient $[W/m^2\ K]$
n	Number of parameters
N	Population size
Nu	Nusselt number
pb	Personal best location of a particle
P_f	Fin pitch [m]
P_l	Longitudinal pitch [m]
P_t	Transverse pitch [m]
Pr	Prandtl number
r_1, r_2	Random numbers
Re	Reynolds number
t	Iteration number
UA	Conductance $\left[\frac{\$\cdot W}{K}\right]$
u_{max}	Maximum velocity of flow
v	Velocity of a particle
w	Inertia weight
x	Location of a particle
δ_f	Fin thickness [m]
κ	Thermal conductivity $[W/m\ K]$
ν	Kinematic viscosity $[m^2/s]$

Subscripts

ex	External flow
min	Minimum
in	Internal flow
i	Current iteration
max	Maximum

Acronyms

CFD	Computational Fluid Dynamics
GA	Genetic Algorithm
HX	Heat exchanger
MT-STHX	Microtube shell-and-tube heat exchanger
PD	Power density $[kW/kg]$
PDTC	Cost-constrained power density
PSO	Particle Swarm Optimization
STHX	Shell-and-tube heat exchanger
sCO_2	Supercritical carbon dioxide

The need to achieve enhanced component designs has produced numerous methodologies to optimize heat transfer processes. Graphical analysis of the search space [29,30], phase-changing optimization design [31], and simulated annealing are among the many methods reported in the past. CFD may be an accurate option to perform optimization studies, but the time costs are heavy [32,33]. Genetic Algorithms (GAs) are frequently used to optimize thermal devices. Caputo et al. [34] computed total cost as a function of capital cost and energy expenditure and performed an economic optimization using a GA. Enforcing pressure drop as a constraint, Selbaş et al. [5] used a GA to obtain optimal design parameters for an STHX. Hilbert et al. [33] performed a GA optimization using direct numerical simulations with multiple objective functions — maximizing heat transfer and minimizing pressure loss.

Though GAs are common, other methods have been reported to overcome the dependence of GAs' optimal solutions on initial conditions. The artificial bee colony algorithm was shown by Sahin et al. [35] to converge much faster than the conventional GA and trial-and-error methods, but this method requires optimal control parameters to avoid premature convergence. Rao et al. [36] and Rao and Patel [37] proposed a teaching–learning based optimization algorithm to decrease the reliance on manual adjustment of parameters. Hadidi et al. [38] developed a design method based on the imperialist competitive algorithm, and later, Hadidi and Nazari [39] developed an approach based on a biology-based algorithm, namely, the biogeography-based optimization algorithm (BBO). Variants of Particle Swarm Optimization (PSO) [40,41] are reliable techniques to perform these optimization studies. Unlike gradient-based algorithms such as the gradient-descent method, PSO is a gradient-free method that does not require gradient information at any point in time. This feature eliminates the need for storage of information that specifies a zero gradient at the saddle point, and thus, PSO is unaffected by discontinuities of the objective function [42,43].

Optimizing the design parameters of HXs to achieve superior performance metrics or targets is critical to the advancement of technology in industrial and aerospace applications. These targets are represented by an objective function and are most commonly the minimization of cost or maximization of heat transfer. Optimization procedures are carried out by defining the objective, a geometric parameter search space, and a set of design constraints [23,44–46]. Common constraints in STHX design ensure that pressure drop does not exceed a given limit and prescribe a minimum value for effectiveness. Then, an iterative trial-and-error computation is performed until a set of optimal design values for the geometric parameters of the heat exchanger is obtained by minimizing or maximizing the objective function within the parameter search space.

Entropy generation [47], entransy generation [48], and field synergy number [49] have been used as objective functions in the past, but the most commonly investigated approach involves the minimization of total cost due to its importance in achieving relevant designs for industrial and aerospace applications [5,35,39]. Estimation of capital cost of STHXs is commonly predicted using the Hall equation, which was developed using the detailed costing procedure for heat exchangers provided by Purohit as a baseline [50]:

$$C_{cap} = a_1 + \left(a_2 \times A_{HT}^{a_3}\right) \tag{1}$$

where A_{HT} is the heat transfer area of the heat exchanger.

However, the Hall equation was developed for STHXs utilizing carbon steel, stainless steel, and titanium as the solid materials. Other costing methods include, but are not limited to, the Pikulik method [51], which can be used for large kettle-type heat exchangers and fixed tube-sheet heat exchangers, the Guthrie method [52] which utilizes heat exchanger surface area to determine capital cost, and the Corripio method [53] which utilizes operating pressure, material used, type of heat exchanger, and surface area to calculate capital cost [54].

An accurate, efficient, and versatile numerical model is essential to conduct optimization studies with multiple parameters. This paper utilizes the correlation-based numerical model developed by Krishna et al. [25–27] to predict thermohydraulic performance of MT-STHXs.

The model is capable of utilizing any working fluid in the CoolProp database [55] and can accurately obtain thermophysical properties of these working fluids at various temperatures and pressures. Any solid material of the user's choice for the MT-STHX can be utilized, and the model has a large application scope.

Current cost models are either applicable to devices with steel as the solid material or are not comprehensive enough to account for the various components of heat exchangers. The objective and novelty of this study is to develop a constrained optimization methodology for MT-STHX design and a related cost model, the form of which can be adapted to MT-STHXs of various configurations and solid materials. Two separate optimization studies are carried out with minimization of capital cost and maximization of power density as objectives. A comparative analysis between cost optimized and power-density optimized MT-STHXs for various MT-STHX capacities is performed to emphasize trade-offs between cost and power density while optimizing within MT-STHX constraints. An additional cost-constrained optimization study is conducted with maximization of power density as the objective to provide a baseline for optimization of future aerospace devices. The proposed optimization objective of maximizing power density while constraining cost is expected to be highly valuable in obtaining practical, optimal designs of thermal devices for aerospace applications. This study utilizes microtubes in STHXs in an effort to obtain cost-effective, highly compact devices and fills an important gap in costing and optimizing sCO_2 heat exchangers for aerospace applications.

2. Particle swarm optimization

PSO is a metaheuristic, gradient-free algorithm initially developed by Kennedy and Eberhart [56,57] and is generally used to optimize non-linear functions. PSO is an evolutionary computation algorithm developed with inspiration from the navigation and foraging of fish schools, bird flocks, and insect swarms [40]. Each individual, known as a particle, interacts with the other particles in the swarm to share essential information and perform complicated tasks collectively or in this case find optimal solutions based on a given objective [58]. Each particle represents a potential solution in an n-dimensional space, where n represents the number of parameters to be optimized [58,59].

In the PSO algorithm, minimum and maximum values of a given parameter are utilized as inputs and an n-dimensional space comprising these parameters is defined as the search space of the problem. Other inputs include the total number of iterations and the population size corresponding to the total number of particles in the swarm. Upon definition of these inputs, each particle in the swarm is initialized at random within the search space, and each particle is given an initial position and velocity value. The fitness of a particle is defined as the value of the objective function which in this study is either the MT-STHX cost or the reciprocal of MT-STHX power density. Solving for the objective function provides a fitness for each particle in the population for the given iteration.

Each particle's velocity and position are updated in the subsequent iteration by utilizing key information from its personal (local) and the population's (global) experience. pb_i is the minimum value of fitness achieved by the given particle (personal best) until the current iteration, and gb is the minimum value of fitness achieved in the entire population (global best) through the current iteration. The velocity of each particle in the subsequent iteration is determined by three factors. Particle velocity representation:

$$v_i(t+1) = c_1 r_1 \left[pb_i(t) - x_i(t)\right] + c_2 r_2 \left[gb(t) - x_i(t)\right] + w v_i(t) \tag{2}$$

Particle position:

$$x_i(t+1) = x_i(t) + v_i(t+1) \tag{3}$$

where t is the current iteration number and i is the particle number. The 1st term in the right side of Eq. (2) is the exploitation term which helps the particles move towards the local optimum. In other words, this term utilizes the personal experience of particles to evaluate the motion of each particle towards its current best location. The 2nd term in Eq. (2) is the exploration term which helps the particles move towards the global optimum. In other words, this term utilizes the experience of the population to evaluate the motion of each particle towards the current global best location. The 3rd term in Eq. (2) is the momentum of the current particle.

w, c_1, and c_2 in Eq. (2) are the key control parameters in the PSO algorithm. Careful selection of these parameters (w, c_1, and c_2) and

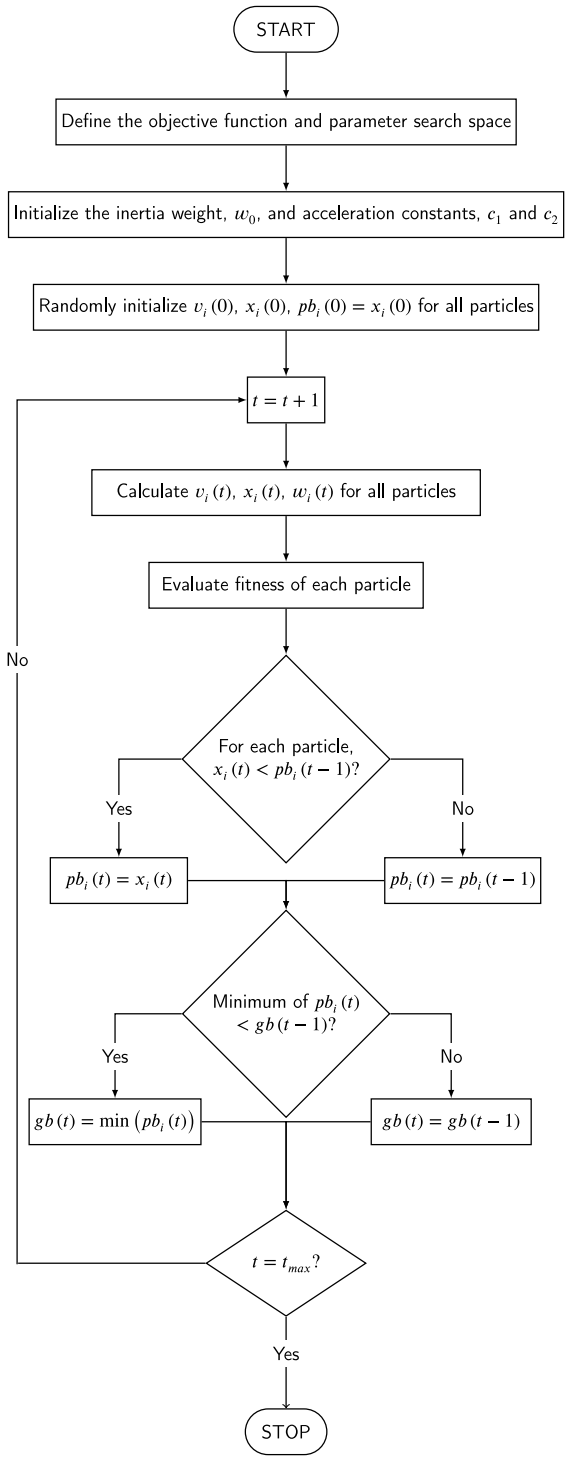

Fig. 1. Flowchart of Particle Swarm Optimization (PSO) algorithm for minimization of an objective function.

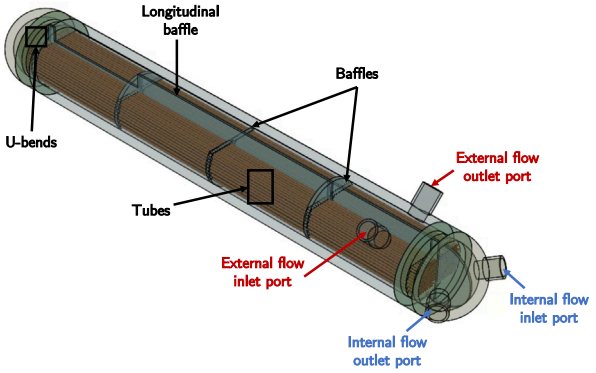

Fig. 2. Isometric view of the MT-STHX geometry in consideration.

maintaining an adequate population size and total number of iterations will ensure that the PSO algorithm reliably predicts a globally optimal solution. w is the inertia weight of the particle and a value of $w > 1$ typically indicates that the particle explores (searches globally) the search space, while a lower value ($w \ll 1$) means that the particle exploits (searches locally) the search space. In the past, researchers typically utilized a constant value of $w = 1$. More recently, others have shown that gradually decreasing w from 0.9 to 0.4 as the iteration number increases produces globally optimal solutions [60,61].

In this paper, inertia weight is decreased linearly as a function of iteration number from 0.9 to 0.4:

$$w_t = \left[\left(w_{max} - w_{min}\right) \times \frac{(t_{max} - t)}{(t_{max})}\right] + w_{min} \tag{4}$$

The values of acceleration constants, c_1 and c_2, govern the extent to which a particle moves towards the personal best or global best. c_1 and c_2 modulate the contributions of the social and cognitive terms, and $c_1 = c_2 = 2$ works well for most applications [56,60,62]. This paper utilizes $c_1 = c_2 = 2$, a population size of $N = 50$, and a total number of iterations of $t_{max} = 1000$. A flowchart of the PSO routine for minimization of an objective function is provided in Fig. 1.

3. Thermohydraulic performance evaluation

The configuration of the MT-STHX modeled here is shown in Fig. 2. The internal flow enters the inlet port and proceeds straight through to the end of the MT-STHX where it encounters U-bends. Internal stream then flows through the U-bends and back to the outlet port where it exits the MT-STHX. The external flow enters the inlet port and flows in a serpentine pattern to the outlet where it exits the MT-STHX. Modeling of the flow streams utilizes the concept of volume averaging to abstract the geometry of the MT-STHX. Details of the numerical model are provided by Krishna et al. [26] and the key equations are summarized below.

The Reynolds number characterizes the flow stream and is essential to compute key parameters such as heat transfer coefficient and pressure drop:

$$Re_{D_h} = \frac{u_{max} D_h}{\nu} \tag{5}$$

where u_{max} is the maximum velocity of flow located at the minimum free flow area, and D_h is the hydraulic diameter which is defined separately for external and internal flows. The hydraulic diameter for the external flow stream is a function of the cross-sectional free flow area between two tubes, A_c, area of heat transfer between two tubes, A_{HT}, and longitudinal pitch, P_l:

$$D_{h_{ex}} = \frac{2A_c P_l}{A_{HT}} \tag{6}$$

For the internal flow stream, hydraulic diameter is simply $D_{h_{in}} = D_{it}$.

Heat transfer coefficients and friction factors for the external flow stream are estimated by utilizing highly accurate correlations developed by Krishna et al. [25]. These correlations take a unified form and can be applied to bare, disc-finned, and cylindrical pin-finned tube banks. External flow heat transfer coefficient and friction factor are obtained as:

$$h_{ex}\frac{D_{h_{ex}}}{\kappa_e \mathrm{Pr}^{\frac{1}{3}}} = 0.47\left(\frac{D_{h_e}}{D_E}\right)^{0.53}\left(\frac{P_t}{D_{ot}}\right)^{-0.21}\left(\frac{P_l}{D_{ot}}\right)^{-0.19}\left(\frac{D_f}{D_{ot}}\right)^{0.12} \times \left(\frac{P_f - \delta_f}{P_f}\right)^{-0.38} Re_{D_{h_{ex}}}^{0.60} \tag{7}$$

$$f_{ex} = 0.54\left(\frac{D_{h_{ex}}}{D_E}\right)^{0.62}\left(\frac{P_t}{D_{ot}}\right)^{0.40}\left(\frac{P_l}{D_{ot}}\right)^{-0.20}\left(\frac{D_f}{D_{ot}}\right)^{-0.45} \times \left(\frac{P_f - \delta_f}{P_f}\right)^{-0.23} Re_{D_{h_{ex}}}^{-0.23} \tag{8}$$

These correlations can be applied within the ranges $0.2 \le \frac{D_{h_{ex}}}{D_E} \le 7.3$, $1.2 \le \frac{P_t}{D_{ot}} \le 3.5$, $1.5 \le \frac{P_l}{D_{ot}} \le 6.0$, $1.0 \le \frac{D_f}{D_{ot}} \le 2.4$, $0.5 \le \frac{P_f - \delta_f}{P_f} \le 1.0$, $1{,}000 \le Re_{D_{h_{ex}}} \le 10{,}000$ and predict heat transfer and friction factor of flow over bare, disc-finned, and cylindrical pin-finned tube banks with less than 7% and 9% average error respectively [25].

The internal flow heat transfer coefficient and friction factor for flow in the turbulent regime are estimated by the Gnielinski equation [63] and Petukhov formula [64], respectively:

$$h_{in} = \frac{\left(f_{in}/8\right)\left(Re_{D_{it}} - 1000\right)\mathrm{Pr}}{1 + 12.7\left(f_{in}/8\right)^{0.5}\left(\mathrm{Pr}^{0.67} - 1\right)}\frac{\kappa_{in}}{D_{it}} \tag{9}$$

$$f_{in} = \left(0.790 \ln Re_{D_{it}} - 1.64\right)^{-2} \tag{10}$$

For flow in the laminar regime, the Nusselt number is $\mathrm{Nu}_{in} = 4.36$, and the friction factor is $f_{in} = 64/Re_{D_{it}}$.

The heat transfer coefficients and friction factors for both flow streams are essential in predicting the thermal and hydraulic performance of the MT-STHX, respectively. Additional correction factors are utilized to account for non-idealities in the flow such as, but not limited to, flow bypass, flow leakage, and contraction and expansion of flow. Discretized forms of the continuity, momentum, and energy equations are iteratively solved to obtain the temperature, flow, and pressure fields within the MT-STHX and in turn, the thermohydraulic performance of the MT-STHX. Further details of the numerical model are provided in Ref. [26], and the computational code utilized in this paper is openly available [27].

4. Cost model

Accurate capital cost estimates of components in the design stages is essential in predicting the feasibility of the component. Modeling of MT-STHXs capital costs involves labor and procurement costs of various subcomponents. The form of the cost model developed in this paper is:

$$C_{cap} = \left[\mathrm{A} \times \text{HX weight [kg]}\right] + \left[\mathrm{B} \times \frac{\text{\# of U-tubes}}{\text{Tube OD [mm]}}\right] + \left[\mathrm{C} \times \text{\# of U-tubes}\right] + \left[\mathrm{D} \times \frac{\text{\# of U-tubes}}{\text{HX length [m]}}\right] + \left[\mathrm{E} \times \text{\# of baffles} \times \text{\# of U-tubes}\right] + \mathrm{F} \tag{11}$$

In Eq. (11), the 1st term on the right side represents the total cost of raw materials which is a function of total MT-STHX weight. The 2nd term provides the cost of tubes; this cost is inversely proportional to the tube OD because the manufacturing cost of tubes of larger diameters is less expensive than that of microtubes. The 3rd, 4th, and 5th terms on the right side of Eq. (11) represent the labor cost of manufacturing or assembly of various components of the MT-STHX. The 3rd term

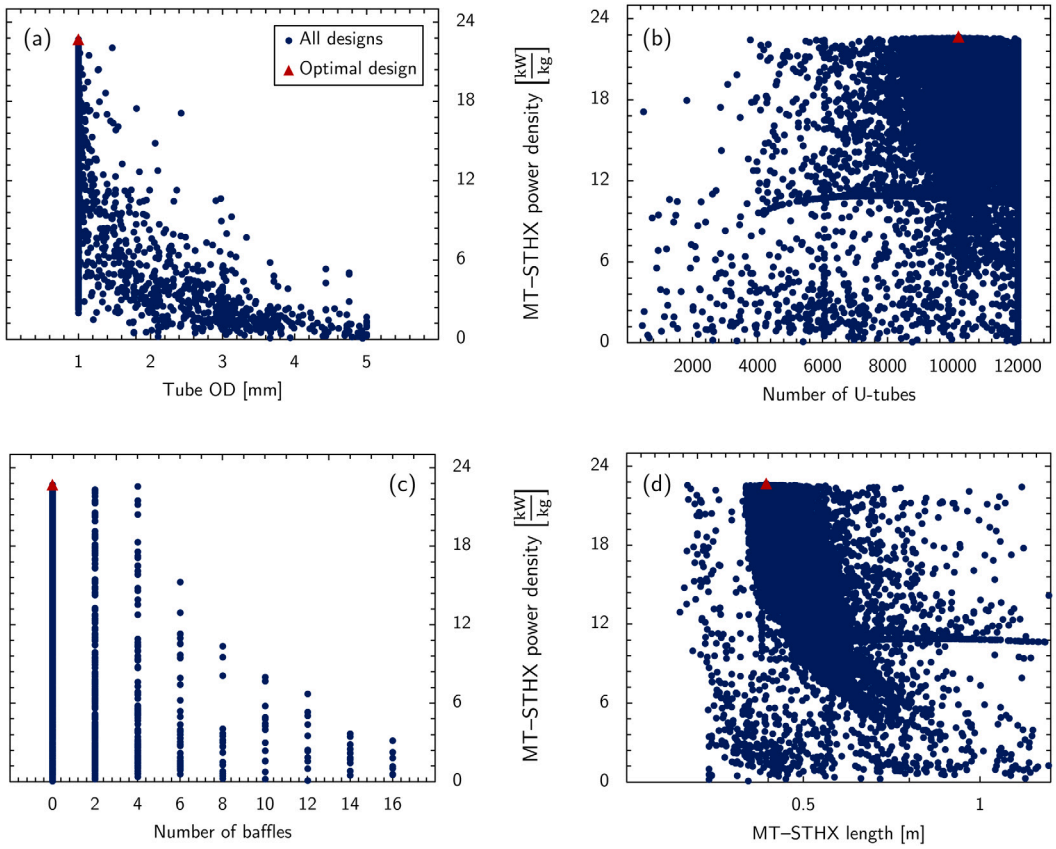

Fig. 3. Demonstration of particle motion in the PSO routine for the 3 MW power-density optimization case.

provides the cost of assembling and joining the tubes to the header, while the 5th term involves the labor cost of slotting the tubes into the baffles. The 4th term provides an estimate for the labor cost of bending the U-tubes while the 6th term captures the fixed costs of manufacturing the shell, longitudinal baffle, sealing strips, manifolds, and ports of the MT-STHX.

The coefficients A through F depend on the configuration of MT-STHX, solid material, and joining processes utilized. Eq. (11) provides a generic form of the cost function to compute capital cost of MT-STHXs, and careful selection of the coefficients can help estimate the cost with an accuracy commensurate with the coefficient uncertainties. The configuration of the MT-STHX shown in Fig. 2 is selected here, and Haynes 282 is utilized as the solid material with supercritical CO_2 as the working fluid for both streams. The values of coefficients A through F would vary based on the intended application, material selection, and manufacturing processes of the STHXs under consideration. For this work, the following values for the coefficients are used to compute MT-STHX total capital cost: A = 255 $/kg, B = 5 $· mm, C = 14 $, D = 2 $·m, E = 2 $, and F = 4000 $.

5. Results and discussion

Heat exchangers designed for use in aerospace applications are optimized with two key objectives in mind: minimization of cost and maximization of power density. Power density is a measure of the waste heat recovered by the HX per unit mass and is given by:

$$\text{HX power density} = \frac{\text{HX capacity [kW]}}{\text{HX weight [kg]}} \tag{12}$$

The total weight of MT-STHXs is computed as a summation of individual components such as the U-tubes, headers, baffles, shell, manifolds, ports, and longitudinal baffle. By utilizing the cost model, two sets of optimization studies have been performed using a PSO routine with minimization of cost (cost optimized) and maximization of power-density (PD-optimized) as the objectives. Optimal designs are obtained for eight MT-STHX capacities ranging from 50 kW to 3 MW. Five design parameters are optimized, and the search space of the problem is provided in Table 1. The mass flow rate is varied to achieve different MT-STHX capacities, and constraints are set to ensure that the pressure drops for both flow streams do not exceed 2% of the inlet value. In order to achieve a given MT-STHX capacity, the MT-STHX length is treated as a floating parameter. With $N = 50$ and $t_{max} = 1000$ as the PSO control parameters, 50,000 MT-STHX designs are searched for each MT-STHX capacity to optimize a given objective before the optimal design is obtained.

Table 1
Parameter search space for the optimizations.

Parameter	Search space
Tube OD [mm]	1.0–5.0
Transverse pitch/Tube OD	1.5–6.0
Longitudinal pitch/Tube OD	1.5–6.0
Number of U-tubes	20–12,000
Number of baffles	0–16

A demonstration of the PSO process is provided in Fig. 3 for the 3 MW power-density optimization case. The figure illustrates the exploration of particles over the entire search space, and as the iterations increase, the particles exploit the search space more locally (closer to the global optimum) in search of the optimal design. A similar trend appears for all the optimization cases and MT-STHX capacities in this study. The search space of all parameters is generally searched continuously except for the number of baffles which is searched discretely in multiples of 2. This is due to the MT-STHX configuration adopted wherein a baffle on one side of the MT-STHX has an accompanying one on the other side of the MT-STHX.

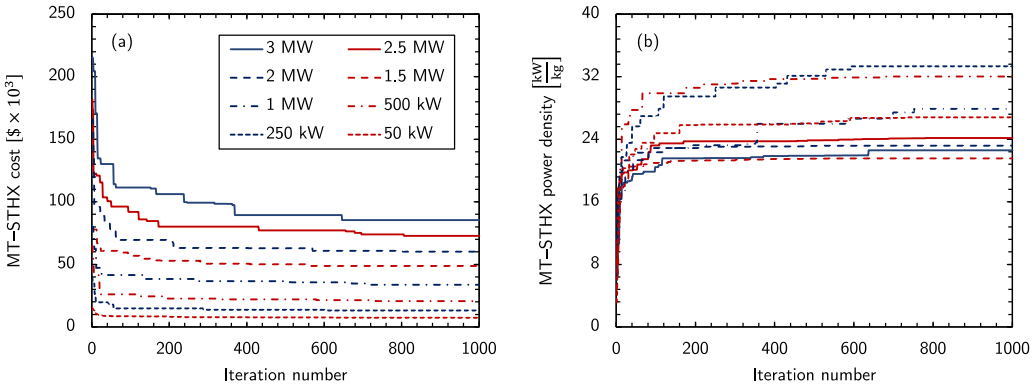

Fig. 4. Convergence of solution for (a) cost optimized and (b) power-density optimized MT-STHX designs.

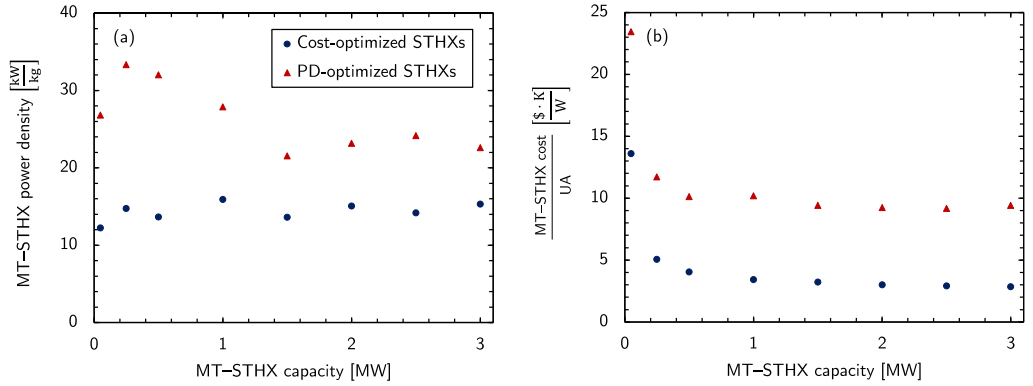

Fig. 5. (a) MT-STHX power density and (b) MT-STHX total cost per UA of the cost optimized and power-density optimized designs as a function of MT-STHX capacity.

Table 2
Design details of the cost optimized MT-STHXs.

Capacity	Tube OD [mm]	Number of U-tubes	MT-STHX length [m]	Number of baffles	Power density [kW/kg]	Cost [$]
50 kW	1.892	36	0.55	14	12.2	6,795
250 kW	2.235	138	0.678	6	14.7	12,684
500 kW	2.32	252	0.772	4	13.6	20,195
1 MW	2.288	520	0.737	4	15.9	34,197
1.5 MW	2.468	730	0.888	2	13.6	48,521
2 MW	2.439	981	0.872	2	15.0	59,986
2.5 MW	2.615	1071	0.944	2	14.2	72,765
3 MW	2.472	1408	0.889	2	15.3	85,417

Solution convergence of the various MT-STHX capacities for both the power density and cost optimization is shown in Fig. 4. All solutions generally converge well with the optimal design not having changed for approx. 300 iterations or more. Geometric details, cost estimate, and performance metrics of the optimal MT-STHX designs for both cost and power-density optimized cases are summarized in Tables 2 and 3. As the capacity of the MT-STHX increases, its estimated capital cost also increases. In order to compare the costs of optimal MT-STHX designs with varying capacities, the cost is normalized by the thermal conductance of the MT-STHX, UA, in units W/K. Conductance is a measure of the ability of the heat exchanger to transfer heat and is a function of the temperatures of both flow streams and the heat transfer rate between the solid material and the two fluid streams.

Fig. 5 provides a comparison of the power density and cost for the various MT-STHX capacities of the power density and cost optimized designs. Table 3 indicates that all power-density optimized designs have a tube OD of 1 mm. As the tube diameter decreases, the volume and weight of the MT-STHXs decreases for a given MT-STHX capacity. Due to the inverse relationship of weight with power density for a given MT-STHX capacity, the power density of the MT-STHX increases. To achieve the same MT-STHX capacity with smaller tube diameters, the number of U-tubes in the MT-STHX must increase to create sufficient area of heat transfer. Increased power density is not always preferred, as the increase in number of tubes corresponds to higher tube manufacturing, procurement, and joining costs. This trend is apparent for both the cost and power-density optimized designs as the number of U-tubes in the optimal designs increase with an increase in the MT-STHX capacities.

The tube diameter of the cost optimized designs is larger than that for the power-density optimized designs. When optimizing for minimization of MT-STHX cost, the expenses incurred by manufacturing, procuring, and joining these tubes need to be minimized. This increase in tube diameter corresponds to a reduction in the number of U-tubes of the optimal MT-STHX of a given thermal capacity as heat transfer area is directly proportional to both tube diameter and number of tubes. A trend common to both sets of optimized designs is that the number of baffles decreases as MT-STHX capacity increases. The power-density optimized designs for MT-STHXs with 1.5 MW capacity and higher have no baffles in the flow stream but contain only one longitudinal baffle. This implies that the external flow has only two shell-side passes — one flow pass perpendicular to the tube bundle on one side of the MT-STHX and another flow pass on the opposite side of the MT-STHX.

Table 3
Design details of the power-density optimized MT-STHXs.

Capacity	Tube OD [mm]	Number of U-tubes	MT-STHX length [m]	Number of baffles	Power density [kW/kg]	Cost [$]
50 kW	1	162	0.206	8	26.8	11,726
250 kW	1	666	0.248	4	33.3	29,283
500 kW	1	1410	0.275	2	32.0	50,674
1 MW	1	2926	0.272	2	27.9	101,998
1.5 MW	1	5063	0.436	0	21.5	141,260
2 MW	1	6650	0.411	0	23.2	184,864
2.5 MW	1	8264	0.396	0	24.2	229,353
3 MW	1	10171	0.395	0	22.6	282,852

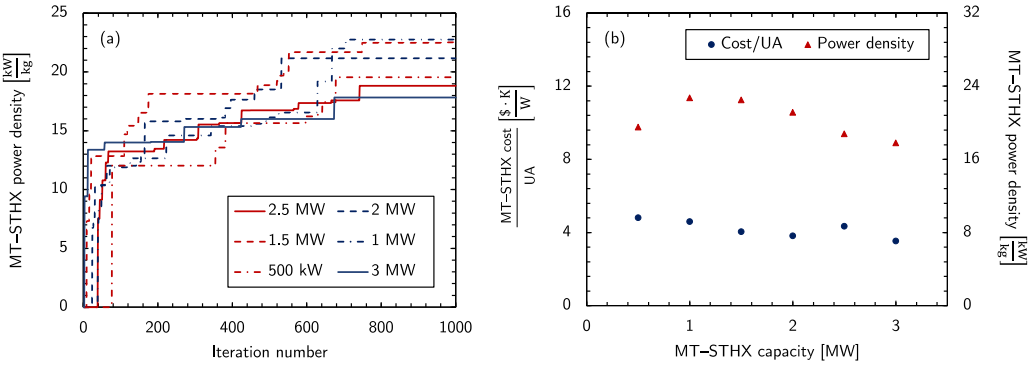

Fig. 6. (a) Convergence of solution for PDTC-optimized MT-STHX designs and (b) MT-STHX power density of the PDTC-optimized designs as a function of MT-STHX capacity.

The power density of the cost optimized designs is around 12–16 kW/kg, with the 1 MW optimal design having the highest power density of 15.9 kW/kg and the 50 kW design having the lowest power density of 12.2 kW/kg. No trend is apparent in the power density of the 50 kW to 1 MW power-density optimal designs, but the power density of the 1.5 MW to 3 MW optimal designs is 21–24 kW/kg. Among the power-density optimal designs, the 250 kW MT-STHX has the highest power density of 33.3 kW/kg, and the 1.5 MW MT-STHX has the lowest power density of about 21.5 kW/kg.

Fig. 5 shows that the optimal MT-STHX cost per conductance follows almost an inverse relationship with MT-STHX capacity for both the cost and power-density optimized designs. The curves peak at the limit case of 50 kW, with the cost optimal design having a MT-STHX cost per conductance of about 14 $\$ \cdot K/W$ and the power-density optimal design having a value of about 23 $\$ \cdot K/W$. The MT-STHX cost per conductance for the larger MT-STHX capacities asymptotes around a specific value for both the cost and power density optimization cases. This value is around 3 $\$ \cdot K/W$ for the cost optimized designs and 9.5 $\$ \cdot K/W$ for the power-density optimized designs.

5.1. Cost-constrained, power density optimization

Even though the power-density optimized designs produce about twice the power for the same weight of the cost optimized designs, their capital cost is also 2- to 3-fold higher. Aerospace applications require highly compact HXs of large capacity, especially in smaller air mobility vehicles where volume and weight demand a premium. Additionally, HXs for any application, or any thermal device, need to be made as cost effectively as possible, given their wide use across many industries. Consequently, co-optimization of power density and cost of HXs is a common goal. To address this issue and to provide a sample optimization to meet this combined objective, a MT-STHX cost per conductance less than $5\$ \cdot K/W$ constraint was set and the MT-STHX designs were optimized with maximization of power density as the objective function. With $N = 50$ and $t_{max} = 1000$, about 50,000 MT-STHX designs were searched, and cost-constrained power-density optimized (PDTC-optimized) designs were obtained for MT-STHX capacities varying from 500 kW to 3 MW. The MT-STHXs with 50 kW and 250 kW capacity are excluded from this case as even the cost optimal designs for these capacities have an MT-STHX cost per conductance greater than $5\$ \cdot K/W$.

Fig. 6 illustrates the solution convergence of the PDTC-optimization case and provides comparisons among the MT-STHX cost per conductance and MT-STHX power density for the various MT-STHX capacities. The MT-STHX cost per conductance is approximately $5\$ \cdot K/W$ for all optimal designs. As implied from the previous optimization cases, the power density of the MT-STHX is inversely proportional to cost. With maximization of power density as the objective, the optimization routine finds the best MT-STHX design at the limit of the MT-STHX cost per conductance constraint. The power densities for all optimal designs fall around 18–23 kW/kg, with the 1 MW MT-STHX having the highest power density of 22.7 kW/kg and the 3 MW MT-STHX having the lowest power density of 17.8 kW/kg. The high values of power density obtained in this paper can be attributed to the utilization of microtubes and sCO_2 as the working fluid.

Table 4 provides the geometric details, cost estimates, and performance metrics of the PDTC-optimized MT-STHX designs. Importantly, geometric parameters such as tube OD, number of U-tubes, and MT-STHX length of the PDTC-optimized MT-STHX designs lie in between those of the PD-optimized and cost optimized MT-STHX designs. Due to the relatively stable value of tube OD near 1.7 mm for all optimal designs, the number of tubes increases with increasing MT-STHX capacity. This trend is maintained to prevent the violation of the pressure drop constraint of the internal flow stream. Aside from the 500 kW design, which consists of four baffles in the flow stream, all other optimal designs have only two baffles and thus a total of four shell-side passes for the external flow stream.

6. Conclusion

This article provides a new multivariate optimization methodology and a generalized equation form to estimate the capital cost of various configurations of microtube shell-and-tube heat exchangers. An accurate and computationally efficient numerical model to predict MT-STHX thermohydraulic performance is utilized in conjunction with the developed cost model to perform multiple optimization studies

Table 4
Design details of the PDTC-optimized MT-STHXs.

Capacity	Tube OD [mm]	Number of U-tubes	MT-STHX length [m]	Number of baffles	Power density [kW/kg]	Cost [$]
500 kW	1.8	470	0.497	4	19.5	24,106
1 MW	1.654	1215	0.462	2	22.7	46,021
1.5 MW	1.618	1625	0.5	2	22.5	60,767
2 MW	1.718	1968	0.542	2	21.2	76,574
2.5 MW	1.655	2833	0.5	2	18.8	108,790
3 MW	1.888	2479	0.616	2	17.8	106,217

with minimization of cost and maximization of power density as the objectives on MT-STHXs utilizing Haynes 282 as the solid material and supercritical CO_2 as the working fluid. The optimization studies carried out have the following highlights:

- MT-STHX designs with power density as high as 33.3 kW/kg for the power density optimized designs and MT-STHX cost per conductance as low as 2.8 $\$ \cdot K/W$ are obtained.
- Despite these promising values, aerospace applications demand HXs to be optimized simultaneously for minimization of cost and maximization of power density. An optimization study is performed by constraining MT-STHX cost per conductance with maximization of power density as the objective. Power densities for these optimal designs are as high as 22 kW/kg when the MT-STHX cost per conductance was constrained to be less than 5 $\$ \cdot K/W$.

This manuscript provides a necessary basis for cost evaluation and optimization of MT-STHXs for utilization in future applications in the aerospace industry. The methodology utilized in this study can be translated and utilized to estimate cost of and optimize other components of thermal power cycles to achieve thermally efficient, highly compact aerospace systems. A potential direction to further this study is utilizing fins on microtubes to achieve higher component power densities. Fins enhance the heat transfer by providing additional heat transfer surface area and in turn reduce volume and weight of the MT-STHX compared to bare tube MT-STHXs with the same capacity. Significant improvements in the processes involved in fabricating bare and finned microtubes would be important in the context of the present study, and feasible bulk manufacturing methods must be developed. This would in turn reduce the cost of manufacturing and procurement of such microtubes and significantly reduce the capital cost of the fabricated MT-STHXs, making them comparable in price to conventional STHXs. With reduced cost of fabricating MT-STHXs, most major drawbacks of conventional STHXs would be addressed, and compact, low-cost, highly efficient thermal cycles in aerospace systems could be realized.

CRediT authorship contribution statement

Akshay Bharadwaj Krishna: Writing – original draft, Conceptualization, Methodology, Software, Formal analysis, Investigation, Visualization. **Kaiyuan Jin:** Writing – review & editing, Conceptualization, Methodology, Supervision. **Portonovo S. Ayyaswamy:** Writing – review & editing, Conceptualization, Methodology, Supervision. **Ivan Catton:** Conceptualization, Methodology, Resources, Supervision. **Timothy S. Fisher:** Writing – review & editing, Conceptualization, Methodology, Funding acquisition, Resources, Supervision.

Declaration of competing interest

The authors declare that they have no known competing financial interests or personal relationships that could have appeared to influence the work reported in this paper.

Data availability

We have cited (ref. Krishna et al. (2022)) a publicly available version of the code used in this work at: http://dx.doi.org/10.5281/zenodo.5117859

Acknowledgments

The authors thank ARPA-E, USA and University of California Los Angeles (UCLA) for their funding, and Dr. Nasr Ghoniem, Dr. Xiaochun Li, Mr. Zachary Wong, and Honeywell Aerospace for their research collaboration and insightful feedback.

Funding

The information, data, or work presented herein was funded in part by the Advanced Research Projects Agency-Energy (ARPA-E), US Dept. of Energy, under Award Number DE-AR0001131, in collaboration with Honeywell Aerospace. The information, data, or work presented herein was funded in part by an agency of the United States Government. Neither the United States Government nor any agency thereof, nor any of their employees, makes any warranty, express or implied, or assumes any legal liability or responsibility for the accuracy, completeness, or usefulness of any information, apparatus, product, or process disclosed, or represents that its use would not infringe privately owned rights. Reference herein to any specific commercial product, process, or service by trade name, trademark, manufacturer, or otherwise does not necessarily constitute or imply its endorsement, recommendation, or favoring by the United States Government or any agency thereof. The views and opinions of authors expressed herein do not necessarily state or reflect those of the United States Government or any agency thereof.

References

[1] J.S. Kwon, S. Son, J.Y. Heo, J.I. Lee, Compact heat exchangers for supercritical CO_2 power cycle application, Energy Convers. Manage. 209 (2020) 112666, http://dx.doi.org/10.1016/j.enconman.2020.112666, URL https://www.sciencedirect.com/science/article/pii/S0196890420302041.

[2] J.F. Hinze, G.F. Nellis, M.H. Anderson, Cost comparison of printed circuit heat exchanger to low cost periodic flow regenerator for use as recuperator in a s-CO_2 Brayton cycle, Appl. Energy 208 (2017) 1150–1161, http://dx.doi.org/10.1016/j.apenergy.2017.09.037.

[3] J. Dyreby, S. Klein, G. Nellis, D. Reindl, Design considerations for supercritical carbon dioxide Brayton cycles with recompression, J. Eng. Gas Turb. Power 136 (10) (2014) http://dx.doi.org/10.1115/1.4027936, URL https://asmedigitalcollection.asme.org/gasturbinespower/article-pdf/136/10/101701/6162213/gtp_136_10_101701.pdf.

[4] B.I. Master, K.S. Chunangad, V. Pushpanathan, Fouling mitigation using helixchanger heat exchangers, in: Proceedings of the ECI Conference on Heat Exchanger Fouling and Cleaning: Fundamentals and Applications, 2003, pp. 317–322.

[5] R. Selbaş, Ö. Kızılkan, M. Reppich, A new design approach for shell-and-tube heat exchangers using genetic algorithms from economic point of view, Chem. Eng. Process.: Process Intensif. 45 (4) (2006) 268–275, http://dx.doi.org/10.1016/j.cep.2005.07.004, URL https://www.sciencedirect.com/science/article/pii/S0255270105001790.

[6] M. Mirzaei, H. Hajabdollahi, H. Fadakar, Multi-objective optimization of shell-and-tube heat exchanger by constructal theory, Appl. Therm. Eng. 125 (2017) 9–19, http://dx.doi.org/10.1016/j.applthermaleng.2017.06.137, URL https://www.sciencedirect.com/science/article/pii/S1359431116343605.

[7] S. Wang, J. Wen, Y. Li, An experimental investigation of heat transfer enhancement for a shell-and-tube heat exchanger, Appl. Therm. Eng. 29 (11) (2009) 2433–2438, http://dx.doi.org/10.1016/j.applthermaleng.2008.12.008, URL https://www.sciencedirect.com/science/article/pii/S1359431108004845.

[8] L. Chordia, M.A. Portnoff, E. Green, High temperature heat exchanger design and fabrication for systems with large pressure differentials, Technical Report, Thar Energy, LLC, Pittsburgh, PA (United States), 2017, http://dx.doi.org/10.2172/1349235.

[9] B. Farajollahi, S.G. Etemad, M. Hojjat, Heat transfer of nanofluids in a shell and tube heat exchanger, Int. J. Heat Mass Transfer 53 (1–3) (2010) 12–17.

[10] R. Lotfi, A.M. Rashidi, A. Amrollahi, Experimental study on the heat transfer enhancement of MWNT-water nanofluid in a shell and tube heat exchanger, Int. Commun. Heat Mass Transfer 39 (1) (2012) 108–111.

[11] M. Mecheri, Y. Le Moullec, Supercritical CO_2 Brayton cycles for coal-fired power plants, Energy 103 (2016) 758–771, http://dx.doi.org/10.1016/j.energy.2016.02.111, URL https://www.sciencedirect.com/science/article/pii/S0360544216301736.

[12] M. Reyes-Belmonte, A. Sebastián, M. Romero, J. González-Aguilar, Optimization of a recompression supercritical carbon dioxide cycle for an innovative central receiver solar power plant, Energy 112 (2016) 17–27, http://dx.doi.org/10.1016/j.energy.2016.06.013, URL https://www.sciencedirect.com/science/article/pii/S0360544216307861.

[13] T. Conboy, S. Wright, J. Pasch, D. Fleming, G. Rochau, R. Fuller, Performance characteristics of an operating supercritical CO_2 Brayton cycle, in: Turbo Expo: Power for Land, Sea, and Air, in: Manufacturing Materials and Metallurgy; Marine; Microturbines and Small Turbomachinery; Supercritical CO_2 Power Cycles, vol. 5, 2012, pp. 941–952, http://dx.doi.org/10.1115/GT2012-68415, URL https://asmedigitalcollection.asme.org/GT/proceedings-pdf/GT2012/44717/941/2417582/941_1.pdf.

[14] H. Miao, Z. Wang, Y. Niu, Performance analysis of cooling system based on improved supercritical CO_2 Brayton cycle for scramjet, Appl. Therm. Eng. 167 (2020) 114774, http://dx.doi.org/10.1016/j.applthermaleng.2019.114774, URL https://www.sciencedirect.com/science/article/pii/S1359431119356601.

[15] J. Syblik, L. Vesely, S. Entler, J. Stepanek, V. Dostal, Analysis of supercritical CO_2 Brayton power cycles in nuclear and fusion energy, Fusion Eng. Des. 146 (2019) 1520–1523, http://dx.doi.org/10.1016/j.fusengdes.2019.02.119, URL https://www.sciencedirect.com/science/article/pii/S0920379619303011.

[16] A.S. Alsagri, A. Chiasson, M. Gadalla, Viability assessment of a concentrated solar power tower with a supercritical CO_2 Brayton cycle power plant, J. Solar Energy Eng. 141 (5) (2019) http://dx.doi.org/10.1115/1.4043515, 051006. URL https://asmedigitalcollection.asme.org/solarenergyengineering/article-pdf/141/5/051006/6411382/sol_141_5_051006.pdf.

[17] T. Ziev, E. Rasouli, I. Noelly-Tano, Z. Wu, S.Y. Rao, N. Lamprinakos, V. Narayanan, A.D. Rollett, P. Vaishnav, Economics of an additive manufactured heat exchanger for concentrating solar power, 2022, Preprint Submitted To EngrXiv.

[18] K.A. Rozman, G. Holcomb, J.A. Hawk, O. Dogan, M. Kapoor, R. Oleksak, J. Kruzic, Performance of Ni-superalloy Haynes 282 with exposure to supercritical gases, 2016, NETL.

[19] K. Kruger, HAYNES 282 alloy, in: Materials for Ultra-Supercritical and Advanced Ultra-Supercritical Power Plants, Elsevier, 2017, pp. 511–545.

[20] S.V. Patankar, D.B. Spalding, A calculation procedure for the transient and steady-state behavior of shell-and-tube heat exchangers, in: Heat Exchangers: Design and Theory Sourcebook, vol. 1, McGraw-Hill New York, 1974.

[21] D. Butterworth, The development of a model for three-dimensional flow in tube bundles, Int. J. Heat Mass Transfer 21 (2) (1978) 253–256, http://dx.doi.org/10.1016/0017-9310(78)90231-4, URL https://www.sciencedirect.com/science/article/pii/0017931078902314.

[22] W.T. Sha, C.I. Yang, T.T. Kao, S.M. Cho, Multidimensional numerical modeling of heat exchangers, J. Heat Transfer 104 (3) (1982) 417–425, http://dx.doi.org/10.1115/1.3245109, URL https://asmedigitalcollection.asme.org/heattransfer/article-pdf/104/3/417/5522001/417_1.pdf.

[23] D.Q. Kern, Process Heat Transfer, vol. 5, McGraw-Hill New York, 1950.

[24] K.J. Bell, Delaware method for shell side design, in: Heat Exchangers-Thermal Hydraulic Fundamentals and Design, Hemisphere Pub, 1981, pp. 581–618.

[25] A.B. Krishna, K. Jin, P.S. Ayyaswamy, I. Catton, T.S. Fisher, Modeling of Supercritical CO_2 Shell-and-Tube Heat Exchangers Under Extreme Conditions. Part I: Correlation Development, J. Heat Transfer 144 (5) (2022) 051902, http://dx.doi.org/10.1115/1.4053510.

[26] A.B. Krishna, K. Jin, P.S. Ayyaswamy, I. Catton, T.S. Fisher, Modeling of Supercritical CO_2 Shell-and-Tube Heat Exchangers Under Extreme Conditions: Part II: Heat Exchanger Model, J. Heat Transfer 144 (5) (2022) 051903, http://dx.doi.org/10.1115/1.4053511.

[27] A.B. Krishna, K. Jin, P.S. Ayyaswamy, I. Catton, T.S. Fisher, akshayb29/Shell-and-Tube-Heat-Exchanger-STHX-numerical-model: Shell-and-tube heat exchanger numerical model, 2021, http://dx.doi.org/10.5281/zenodo.5117859.

[28] K. Jin, A.B. Krishna, Z. Wong, P. Ayyaswamy, I. Catton, T.S. Fisher, Thermo-hydraulic experiments on a supercritical carbon dioxide - air microtube heat exchanger, 2022, Under Review.

[29] K. Muralikrishna, U. Shenoy, Heat exchanger design targets for minimum area and cost, Chem. Eng. Res. Des. 78 (2) (2000) 161–167, http://dx.doi.org/10.1205/026387600527185, URL https://www.sciencedirect.com/science/article/pii/S0263876200718788.

[30] T. Poddar, G. Polley, Heat exchanger design through parameter plotting, Chem. Eng. Res. Des. 74 (8) (1996) 849–852.

[31] B. Allen, L. Gosselin, Optimal geometry and flow arrangement for minimizing the cost of shell-and-tube condensers, Int. J. Energy Res. 32 (10) (2008) 958–969, http://dx.doi.org/10.1002/er.1398, URL https://onlinelibrary.wiley.com/doi/abs/10.1002/er.1398.

[32] K. Foli, T. Okabe, M. Olhofer, Y. Jin, B. Sendhoff, Optimization of micro heat exchanger: CFD, analytical approach and multi-objective evolutionary algorithms, Int. J. Heat Mass Transfer 49 (5–6) (2006) 1090–1099, http://dx.doi.org/10.1016/j.ijheatmasstransfer.2005.08.032.

[33] R. Hilbert, G. Janiga, R. Baron, D. Thévenin, Multi-objective shape optimization of a heat exchanger using parallel genetic algorithms, Int. J. Heat Mass Transfer 49 (15) (2006) 2567–2577, http://dx.doi.org/10.1016/j.ijheatmasstransfer.2005.12.015, URL https://www.sciencedirect.com/science/article/pii/S0017931006000822.

[34] A.C. Caputo, P.M. Pelagagge, P. Salini, Heat exchanger design based on economic optimisation, Appl. Therm. Eng. 28 (10) (2008) 1151–1159, http://dx.doi.org/10.1016/j.applthermaleng.2007.08.010, URL https://www.sciencedirect.com/science/article/pii/S1359431107002839.

[35] A. Şencan Şahin, B.K. lıç, U.K. lıç, Design and economic optimization of shell and tube heat exchangers using Artificial Bee Colony (ABC) algorithm, Energy Convers. Manage. 52 (11) (2011) 3356–3362, http://dx.doi.org/10.1016/j.enconman.2011.07.003, URL https://www.sciencedirect.com/science/article/pii/S0196890411001944.

[36] R. Rao, V. Savsani, D. Vakharia, Teaching–learning-based optimization: An optimization method for continuous non-linear large scale problems, Inform. Sci. 183 (1) (2012) 1–15, http://dx.doi.org/10.1016/j.ins.2011.08.006, URL https://www.sciencedirect.com/science/article/pii/S0020025511004191.

[37] R.V. Rao, V. Patel, Multi-objective optimization of heat exchangers using a modified teaching-learning-based optimization algorithm, Appl. Math. Model. 37 (3) (2013) 1147–1162, http://dx.doi.org/10.1016/j.apm.2012.03.043, URL https://www.sciencedirect.com/science/article/pii/S0307904X12002065.

[38] A. Hadidi, M. Hadidi, A. Nazari, A new design approach for shell-and-tube heat exchangers using imperialist competitive algorithm (ICA) from economic point of view, Energy Convers. Manage. 67 (2013) 66–74, http://dx.doi.org/10.1016/j.enconman.2012.11.017, URL https://www.sciencedirect.com/science/article/pii/S0196890412004530.

[39] A. Hadidi, A. Nazari, Design and economic optimization of shell-and-tube heat exchangers using biogeography-based (BBO) algorithm, Appl. Therm. Eng. 51 (1) (2013) 1263–1272, http://dx.doi.org/10.1016/j.applthermaleng.2012.12.002, URL https://www.sciencedirect.com/science/article/pii/S1359431112008071.

[40] V. Patel, R. Rao, Design optimization of shell-and-tube heat exchanger using particle swarm optimization technique, Appl. Therm. Eng. 30 (11) (2010) 1417–1425, http://dx.doi.org/10.1016/j.applthermaleng.2010.03.001, URL https://www.sciencedirect.com/science/article/pii/S1359431110001080.

[41] V.C. Mariani, A.R.K. Duck, F.A. Guerra, L. dos Santos Coelho, R.V. Rao, A chaotic quantum-behaved particle swarm approach applied to optimization of heat exchangers, Appl. Therm. Eng. 42 (2012) 119–128, http://dx.doi.org/10.1016/j.applthermaleng.2012.03.022, URL https://www.sciencedirect.com/science/article/pii/S1359431112001913.

[42] E.C. Laskari, K.E. Parsopoulos, M.N. Vrahatis, Particle swarm optimization for minimax problems, in: Proceedings of the 2002 Congress on Evolutionary Computation. CEC'02 (Cat. No. 02TH8600), vol. 2, IEEE, 2002, pp. 1576–1581.

[43] R. Ge, F. Huang, C. Jin, Y. Yuan, Escaping from saddle points—online stochastic gradient for tensor decomposition, in: Conference on Learning Theory, PMLR, 2015, pp. 797–842.

[44] R. Shah, K. Bell, CRC Handbook of Thermal Engineering, CRC Press, Boca Raton, Florida, 2000.

[45] W.M. Rohsenow, J.P. Hartnett, Y.I. Cho, et al., Handbook of Heat Transfer, vol. 3, McGraw-Hill New York, 1998.

[46] G.F. Hewitt, Heat Exchanger Design Handbook, Begell House, 1998.

[47] J. Guo, L. Cheng, M. Xu, Optimization design of shell-and-tube heat exchanger by entropy generation minimization and genetic algorithm, Appl. Therm. Eng. 29 (14) (2009) 2954–2960, http://dx.doi.org/10.1016/j.applthermaleng.2009.03.011, URL https://www.sciencedirect.com/science/article/pii/S1359431109000921.

[48] J. Guo, L. Cheng, M. Xu, Entransy dissipation number and its application to heat exchanger performance evaluation, Chin. Sci. Bull. 54 (15) (2009) 2708–2713.

[49] J. Guo, M. Xu, L. Cheng, The application of field synergy number in shell-and-tube heat exchanger optimization design, Appl. Energy 86 (10) (2009) 2079–2087, http://dx.doi.org/10.1016/j.apenergy.2009.01.013, URL https://www.sciencedirect.com/science/article/pii/S0306261909000257.

[50] G.P. Purohit, Estimating costs of shell-and-tube heat exchangers, Chem. Eng. 90 (17) (1983) 56–67.

[51] A. Pikulik, H.E. Diaz, Cost estimating for major process equipment, Chem. Eng. (1977) 106–122.

[52] K.M. Guthrie, Capital cost estimating, modern cost engineering techniques, Chem. Eng. (1969) 114–142.
[53] A.B. Corripio, K.S. Chrien, L.B. Evans, Estimate costs of heat exchangers and storage tanks via correlations, Chem. Eng. Mag. Mod. Cost Eng. II (1984) 144–146.
[54] M. Taal, I. Bulatov, J. Klemeš, P. Stehlık, Cost estimation and energy price forecasts for economic evaluation of retrofit projects, Appl. Therm. Eng. 23 (14) (2003) 1819–1835, http://dx.doi.org/10.1016/S1359-4311(03)00136-4, URL https://www.sciencedirect.com/science/article/pii/S1359431103001364.
[55] I.H. Bell, J. Wronski, S. Quoilin, V. Lemort, Pure and pseudo-pure fluid thermophysical property evaluation and the open-source thermophysical property library CoolProp, Ind. Eng. Chem. Res. 53 (6) (2014) 2498–2508.
[56] J. Kennedy, R. Eberhart, Particle swarm optimization, in: Proceedings of ICNN'95-International Conference on Neural Networks, vol. 4, IEEE, 1995, pp. 1942–1948.
[57] R. Eberhart, J. Kennedy, A new optimizer using particle swarm theory, in: MHS'95. Proceedings of the Sixth International Symposium on Micro Machine and Human Science, IEEE, 1995, pp. 39–43.
[58] H. Zhu, Y. Wang, K. Wang, Y. Chen, Particle Swarm Optimization (PSO) for the constrained portfolio optimization problem, Expert Syst. Appl. 38 (8) (2011) 10161–10169, http://dx.doi.org/10.1016/j.eswa.2011.02.075, URL https://www.sciencedirect.com/science/article/pii/S0957417411002818.
[59] H. Garg, A hybrid PSO-GA algorithm for constrained optimization problems, Appl. Math. Comput. 274 (2016) 292–305, http://dx.doi.org/10.1016/j.amc.2015.11.001, URL https://www.sciencedirect.com/science/article/pii/S0096300315014630.
[60] S. Sengupta, S. Basak, R.A. Peters, Particle swarm optimization: A survey of historical and recent developments with hybridization perspectives, Mach. Learn. Knowl. Extract. 1 (1) (2019) 157–191.
[61] J.C. Bansal, P. Singh, M. Saraswat, A. Verma, S.S. Jadon, A. Abraham, Inertia weight strategies in particle swarm optimization, in: 2011 Third World Congress on Nature and Biologically Inspired Computing, IEEE, 2011, pp. 633–640.
[62] F. Marini, B. Walczak, Particle swarm optimization (PSO). A tutorial, Chemometr. Intell. Lab. Syst. 149 (2015) 153–165, http://dx.doi.org/10.1016/j.chemolab.2015.08.020, URL https://www.sciencedirect.com/science/article/pii/S0169743915002117.
[63] V. Gnielinski, New equations for heat and mass transfer in turbulent pipe and channel flow, Int. Chem. Eng. 16 (2) (1976) 359–368.
[64] B. Petukhov, Heat transfer and friction in turbulent pipe flow with variable physical properties, in: Advances in Heat Transfer, vol. 6, Elsevier, 1970, pp. 503–564.